Available online at www.sciencedirect.com

ScienceDirect

Geochimica et Cosmochimica Acta 121 (2013) 452–466

Geochimica et Cosmochimica Acta

www.elsevier.com/locate/gca

The oxygen isotope evolution of parent body aqueous solutions as recorded by multiple carbonate generations in the Lonewolf Nunataks 94101 CM2 carbonaceous chondrite

M.R. Lee [a], M.R. Sofe [a], P. Lindgren [a,*], N.A. Starkey [b], I.A. Franchi [b]

[a] School of Geographical and Earth Sciences, University of Glasgow, Gregory Building, Lilybank Gardens, Glasgow G12 8QQ, UK
[b] Planetary & Space Sciences, The Open University, Milton Keynes MK7 6AA, UK

Received 19 February 2013; accepted in revised form 9 July 2013; available online 19 July 2013

Abstract

The CM2 carbonaceous chondrite LON 94101 contains aragonite and two generations of calcite that provide snapshots of the chemical and isotopic evolution of aqueous solutions during parent body alteration. Aragonite was the first carbonate to crystallize. It is rare, heterogeneously distributed within the meteorite matrix, and its mean oxygen isotope values are $\delta^{18}O$ $39.9 \pm 0.6‰$, $\Delta^{17}O$ $-0.3 \pm 1.0‰$ (1σ). Calcite precipitated soon afterwards, and following a fall in solution Mg/Ca ratios, to produce small equant grains with a mean oxygen isotope value of $\delta^{18}O$ $37.5 \pm 0.7‰$, $\Delta^{17}O$ $1.4 \pm 1.1‰$ (1σ). These grains were partially or completely replaced by serpentine and tochilinite prior to precipitation of the second generation of calcite, which occluded an open fracture to form a millimetre-sized vein, and replaced anhydrous silicates within chondrules and the matrix. The vein calcite has a mean composition of $\delta^{18}O$ $18.4 \pm 0.3‰$, $\Delta^{17}O$ $-0.5 \pm 0.5‰$ (1σ). Petrographic and isotopic results therefore reveal two discrete episodes of mineralisation that produced calcite generations with contrasting $\delta^{18}O$, and mean $\Delta^{17}O$ values. The aragonite and equant calcite crystallized over a relatively brief period early in the aqueous alteration history of the parent body, and from static fluids that were evolving chemically in response to mineral dissolution and precipitation. The second calcite generation crystallized from solutions of a lower $\Delta^{17}O$, and a lower $\delta^{18}O$ and/or higher temperature. As two generations of calcite whose petrographic characteristics and oxygen isotopic compositions are similar to those in LON 94101 occur in at least one other CM2, multiphase carbonate mineralisation could be the typical outcome of the sequence of chemical reactions during parent body aqueous alteration. It is equally possible however that the second generation of calcite formed in response to an event such as impact fracturing and concomitant fluid mobilisation that affected a large region of the common parent body of several CM2 meteorites. These findings show that integrated petrographic, chemical and isotopic studies can provide new insights into the mechanisms of parent body alteration including the spatial and temporal dynamics of the aqueous system.

1. INTRODUCTION

The CM carbonaceous chondrites contain minerals including phyllosilicates and carbonates that formed by parent body aqueous alteration (DuFresne and Anders, 1962). The liquid water must have been generated by melting of H_2O ice accompanying heating of the parent body, but the mechanisms by which aqueous fluids interacted with primary anhydrous minerals to form the alteration products remain controversial. A key question is whether aqueous solutions were chemically closed or open on length scales greater than that of a meteorite (i.e. $>\sim$1 m). The closed system models (e.g. DuFresne and Anders, 1962; Clayton and Mayeda, 1999; Rubin et al., 2007) require that fluids were essentially static, probably owing to the very low permeability of parent body interiors (Bland et al., 2009). These models are consistent with the unfractionated bulk chemical

* Corresponding author. Tel.: +44 1413305442.
E-mail address: paula.lindgren@glasgow.ac.uk (P. Lindgren).

0016-7037/$ - see front matter © 2013 Published by Elsevier Ltd.
http://dx.doi.org/10.1016/j.gca.2013.07.010

compositions of carbonaceous chondrites, and interpretations of oxygen isotope analysis of bulk meteorites and their components (e.g. DuFresne and Anders, 1962; Clayton and Mayeda, 1984, 1999). However, the oxygen isotope evidence can also support models that posit a chemically open system with fluid flow (Young et al., 1999; Young, 2001), and they are supported by numerical simulations of parent body evolution (e.g. Young et al., 2003; Travis and Schubert, 2005; Palguta et al., 2010). Determining which of these models best describes water-mediated alteration of parent body interiors is very important for our understanding of the chronology and drivers of early solar system processes, and the present-day internal structure and composition of asteroids and comets.

As a means of obtaining evidence to help discriminate between closed and open system models, we have sought to understand better the dynamics of the aqueous system on both intra- and inter-meteorite length scales. Our work has focused on carbonates because their mineralogy and chemistry provides a record of the major and trace element composition, pH and Eh of ambient solutions (e.g. Johnson and Prinz, 1993; Riciputi et al., 1994; Brearley, 1998), and their oxygen isotope ratios contain information on the temperature and provenance of the fluids (Benedix et al., 2003; Guo and Eiler, 2007; Tyra et al., 2007, 2012). Grain microstructures can also reveal the intensity of parent body deformation during and after aqueous alteration (Lee and Ellen, 2008; Lindgren et al., 2011). As carbonate crystallization ages can be determined using the ^{53}Mn–^{53}Cr system (Brearley and Hutcheon, 2000, 2002; Brearley et al., 2001; de Leuw et al., 2009; Fujiya et al., 2012; Lee et al., 2012), the information on fluid evolution and parent body stress histories that these minerals provide can be interpreted within the framework of an absolute chronology.

Early studies of CM carbonates found limited mineralogical and chemical variations within and between meteorites (Johnson and Prinz, 1993; Riciputi et al., 1994), which would be consistent with a brief episode of crystal growth within a system that was chemically closed on length scales greater than that of a meteorite. However, subsequent petrographic, mineralogical and chemical studies have described multiple generations of carbonates within individual meteorites, and mineralisation histories that differ greatly between CMs. These findings point towards an aqueous system that was temporally dynamic and spatially variable (Benedix et al., 2003; Rubin et al., 2007; Lee and Ellen, 2008; de Leuw et al., 2010; Lindgren et al., 2011, 2012; Lee et al., 2012). Most recently Tyra et al. (2012) described two generations of pre-terrestrial calcite in the paired Antarctic meteorites EET 96006, EET 96016, EET 96017, EET 96019 (hereafter 'EET 96006-paired') that differ in their petrographic characteristics and oxygen isotope values. They concluded that the two generations had crystallized at different times from a fluid that was becoming isotopically lighter as it acquired ^{16}O by reaction with primary anhydrous silicates. Tyra et al. (2012) further suggested that isotopically distinct carbonate generations may be present in other CM2 meteorites. If this hypothesis of episodic carbonate mineralisation throughout the CM2 parent body or bodies can be confirmed, it has important implications for our understanding of the interconnectivity of the aqueous system and drivers of fluid evolution.

Lonewolf Nunataks (LON) 94101 is an Antarctic CM2 find that contains two petrographically distinct generations of calcite together with grains of aragonite that are up to 100 μm in size and so are much coarser than those in most other CM2s (Lee and Ellen, 2008). As the relative ages of the two calcite generations have been previously determined (Lindgren et al., 2011), LON 94101 provides an opportunity to ask whether their direction of oxygen isotope evolution described by Tyra et al. (2012) (i.e. both $\delta^{17}O$ and $\delta^{18}O$ decreasing with time) is common to other CM2s. Here the oxygen isotope values of all three generations of Ca-carbonate in LON 94101 have been determined by NanoSIMS, and their petrographic relationships and chemical compositions have been documented by electron imaging and X-ray microanalysis. In addition to understanding the relative chronology and length scale of the isotopic evolution of parent body solutions, this study has also sought to discover the provenance of the calcium and bicarbonate ions that formed the calcite, and the reasons why Ca-carbonate crystallized in three discrete episodes.

2. MATERIALS AND METHODS

2.1. Petrographic and mineralogical characterisation of LON 94101

LON 94101 is a 2804.6 g CM2 carbonaceous chondrite that was recovered by the US Antarctic Search for Meteorites program (ANSMET) in 1994. The meteorite has a moderate weathering grade (Be) and contains abundant fractures (fracturing category C) (AMN 18(2), 1995). Using the scheme of Rubin et al. (2007), LON 94101 can be classified as a CM 2.2–2.3. For this study one polished thin section was used (LON 94101, 50), and the rock slice is roughly rectangular in shape (Lindgren et al., 2011).

Following coating with carbon, the thin section was studied by backscattered electron (BSE) imaging and energy-dispersive X-ray (EDX) mapping using a FEI Quanta 200F field-emission scanning electron microscope (SEM) equipped with an EDAX Genesis microanalysis system and a KE Developments cathodoluminescence (CL) detector. The SEM was operated at high vacuum, with an accelerating voltage of 20 kV, and a relatively high beam current (current is not quantified on this instrument). The abundances of various constituents of the meteorite (i.e. carbonate grains, matrix, chondrules, etc.) were determined by SEM point counting, whereby the sample is systematically traversed (using the frame-by-frame stage movement function), and the material in the center of the field of view after each stage movement is identified. Carbonate grains are described with reference to their size (expressed as the longest dimension), and their shape. LON 94101 contains both aragonite and calcite, and these two Ca-carbonate polymorphs were distinguished using a Renishaw inVia Raman microscope operated with a 514 nm laser that has a spot size of ~1 μm. The dominant Raman band of both minerals is at ~1085 cm^{-1}, which is due to the symmetric stretching (ν_1)

vibration of CO_3^{2-}. However, as the two minerals differ in their crystal structure, they can be distinguished using the position of some of their minor Raman bands. Aragonite has minor bands at ~207 and 704 cm^{-1}, and calcite at ~282 and 713 cm^{-1} (White, 2009).

2.2. X-ray microanalysis

The chemical compositions of Ca-carbonate grains were quantified by electron probe microanalysis (EPMA) using a five spectrometer Cameca SX100 instrument at the University of Edinburgh. It was operated at 15 kV/3 nA for determination of Ca and 15 kV/20 nA for Na, Mg, Mn, Fe and Sr; the spot size was ~5 μm. Calibration used the following standards: jadeite (Na), spinel (Mg), calcite (Ca), Mn metal (Mn), fayalite (Fe) and celestite (Sr). Average detection limits were 0.01 wt% Mg, 0.04 wt% Na, Fe and Sr, and 0.05 wt% Mn. Datapoints with anomalously high Mg and/or Fe concentrations were discarded as they likely reflect contamination of the analysed volume by phyllosilicates. This filtering could have been undertaken with more confidence if Si was also analysed for, but this was not attempted owing to contamination of Ca-carbonate grains by colloidal silica, which had been used to polish them for earlier Electron Backscatter Diffraction (EBSD) work (Lindgren et al., 2011).

The calcite grains are frequently associated with patches of intergrown serpentine and tochilinite, whose compositions were also determined by EPMA. Two conditions were used in each analysis (both with a spot size of ~5 μm): 15 kV/2 nA (for Na, Mg Al, Si, Ca, Fe) and 15 kV/20 nA (for P, S, K, Ti, Cr, Mn, Ni). Calibration used the following standards: jadeite (Na), spinel (Mg, Al), wollastonite (Si, Ca), apatite (P), pyrite (S), orthoclase (K), rutile (Ti), Cr metal (Cr), Mn metal (Mn), fayalite (Fe) and Ni metal (Ni). Average detection limits were: 0.01 wt% K, 0.02 wt% P and Ti, 0.03 wt% S, 0.04 wt% Cr, 0.05 wt% Mg and Ni, 0.06 wt% Na, 0.07 wt% Al and Ca, 0.10 wt% Si, 0.13 wt% Mn and 0.19 wt% Fe.

2.3. Determination of oxygen isotope compositions by NanoSIMS

Oxygen isotope analyses were obtained from grains of calcite and aragonite using a NanoSIMS 50L at the Open University, UK. These analyses were performed in 'spot' mode, whereby the focussed primary beam was rastered over a small area and the total ion signal integrated. A Cs^+ ion beam with a current of ~30 pA (~60 pA for pre-sputter) was used, with ^{16}O measured on a Faraday cup and ^{17}O and ^{18}O on electron multipliers. $^{24}Mg^{16}O$, $^{40}Ca^{16}O$ and $^{56}Fe^{16}O$ were also measured on electron multipliers to monitor relative mineral compositions. The mass resolving power was set to >10,000 (Cameca NanoSIMS definition, based on the measured peak width containing 80% of the ion beam), which was sufficient to resolve the interference of ^{16}OH on the ^{17}O peak. Charge compensation was applied using the electron gun. Areas for analysis were 5 × 5 μm, with a larger area for pre-sputter (7 × 7 μm) in order to implant Cs ions evenly and reach sputter equilibrium across the area to be analysed. Analysis times, including pre-sputter, were typically ~8 min with total counts of ^{16}O in a single analysis being 1×10^9.

Isotope ratios were normalised to Standard Mean Ocean Water (SMOW) using analyses of a calcite or aragonite standard that bracketed the sample analyses in order to generate $\delta^{17}O$ and $\delta^{18}O$ values, and also to provide corrections for instrumental mass fractionation. The errors quoted combine internal errors for each analysis with the standard deviation of the mean of the associated standards. Calcite analyses used an internal calcite standard with a composition of $\delta^{18}O = 15.47 \pm 0.07$ (1σ) ‰ VSMOW that was determined from replicate analyses ($n = 6$) on a Thermo Gasbench II connected to a Delta Advantage mass spectrometer in Planetary and Space Sciences at the Open University. For these measurements powdered aliquots were reacted with anhydrous H_3PO_4 at 72 ± 0.1 °C for 1 h. The CO_2 generated from this reaction was then flushed from the head-space of the reaction vessel, dried through Nafian traps before passing through a Poraplot Q fused silica capillary column to separate other possible contaminants prior to analysis on the mass spectrometer. Aragonite analyses were calibrated against a sample of Kygole aragonite that was obtained from the Hunterian Museum, Glasgow (specimen number GLAHM 134627). Its $\delta^{18}O$ value of 27.49 ± 0.15 (1σ) ‰ VSMOW was determined from 6 replicate analyses of 1 mg powdered sub-samples. Each sub-sample was reacted with anhydrous H_3PO_4 at 70 ± 0.1 °C for 1 h to produce CO_2, and $\delta^{18}O_{VSMOW}$ was then determined using an AP2003 continuous-flow mass spectrometer. Analyses of the aragonite samples were interspersed with international calcite standards NBS18, NBS19 and internal laboratory standards for calibration and corrections. For the standards, $\delta^{17}O$ was assumed to lie on the terrestrial fractionation line (TFL; defined as $\delta^{17}O = 0.52 \times \delta^{18}O$). Analyses of ≈10 NanoSIMS measurements of calcite and aragonite standards show that reproducibility of $\delta^{18}O$ was ±1.2–1.4‰ (2σ) and for $\Delta^{17}O$ was ±1.2–2.1‰ (2σ). The sample and standards were positioned in separate blocks mounted on the same sample holder. Using identical analytical procedures to those presented here, Starkey and Franchi (2013) found no statistically significant variation in oxygen isotope ratios when measuring polished samples of San Carlos olivine mounted in different positions across the NanoSIMS holder (up to 40 mm distance apart). NanoSIMS results are expressed as $\delta^{17}O$, $\delta^{18}O$ and $\Delta^{17}O$ (i.e. $\delta^{17}O - 0.52\ \delta^{18}O$), which is a measure of departure from the TFL.

3. RESULTS

3.1. Petrography of LON 94101

The thin section studied is unbrecciated and lacks clasts, although other samples of the LON 94101 meteorite contain clasts of a variety of petrologic types (Lindgren et al., 2013). It is composed of chondrules with fine-grained

rims that are supported within a fine-grained matrix. SEM point counting shows that Ca-carbonate comprises 1.3 vol.% of the thin section, and four petrographically distinct varieties have been identified: (i) grains of aragonite within the matrix, (ii) equant grains of calcite within the matrix, (iii) a millimetre-sized calcite vein that cross-cuts the matrix, and (iv) micropore-rich calcite intergrown with anhydrous silicate grains that are present in the matrix and within chondrules. The carbonates are not distributed uniformly, and two regions of the thin section can be identified. In the 'AEC-rich' region aragonite and equant calcite grains are abundant, whereas in the 'AEC-poor' region they are rare (Fig. 1). These two regions can be readily identified on a Ca X-ray map despite their gradational boundaries (Fig. 1b), but no clear differences between them are apparent in BSE images (Fig. 1a). The calcite vein occurs at the boundary between the two regions, and the largest calcite-bearing chondrules are found in the AEC-poor part (Fig. 1b). The four varieties of carbonates are described below in order of their inferred sequence of crystallization.z

3.2. Aragonite grains

Twenty nine grains of aragonite were identified in the meteorite matrix. The thin section has an overall aragonite abundance of 0.21 grains mm^{-2}, although only 3 grains occur in the AEC-poor region (Fig. 1c). The aragonite grains range in size from 5 to 100 μm (mean of 29 μm). All of them have pores along their contact with the matrix and many also contain irregular intracrystalline pores and fractures (Fig. 2a and b). Aragonite has a mean chemical composition of $Ca_{99.03}Mg_{0.13}Fe_{0.77}Sr_{0.07}CO_3$ ($n = 12$, Table 1), and its oxygen isotopic composition is $\delta^{18}O$ 39.9 ± 0.6‰, $\Delta^{17}O$ −0.3 ± 1.0‰ (1σ) ($n = 6$, Table 2).

3.3. Equant calcite grains

Equant calcite is the most abundant of the four varieties of Ca-carbonate, although grains are heterogeneously distributed and scarce in the AEC-poor region (Fig. 1b). The twenty five grains measured range in size from 9 to 51 μm, with a mean of 26 μm. They are monocrystalline

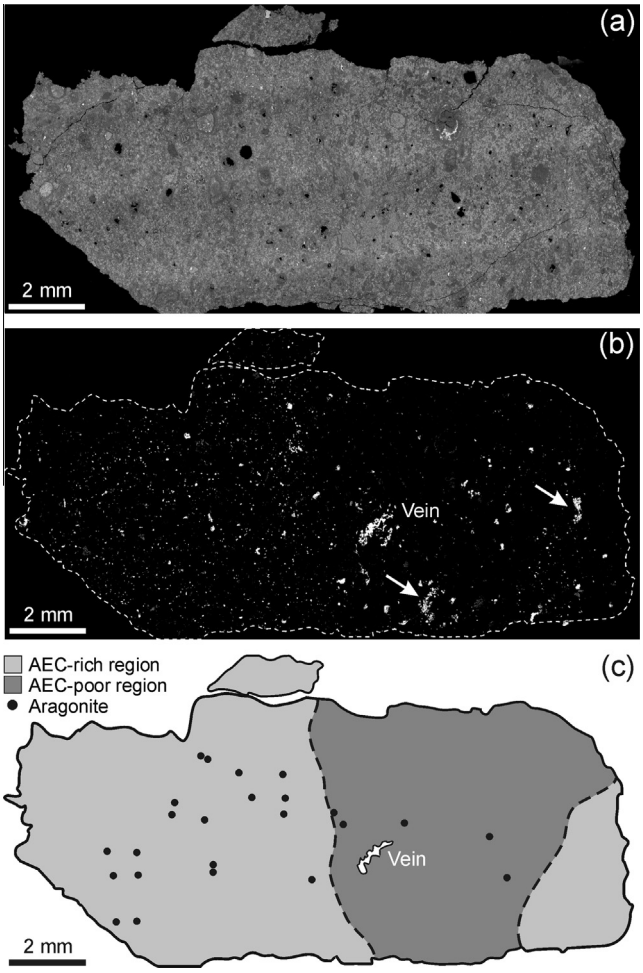

Fig. 1. The LON 94101 thin section. (a) BSE image. (b) Ca K_α X-ray map highlighting Ca-carbonate (white). The smallest Ca-carbonate grains are aragonite and equant calcite, which are most numerous in the AEC-rich region. Coarser areas of Ca-carbonate occur within chondrules, some of which are arrowed, and they are concentrated in the AEC-poor region. The calcite vein is indicated, and the edges of the thin section are delineated by a dashed white line. (c) Diagram showing the distribution within the thin section of the AEC-poor and AEC-rich regions and the locations of the aragonite grains, some of which are too close to label individually, and the calcite vein.

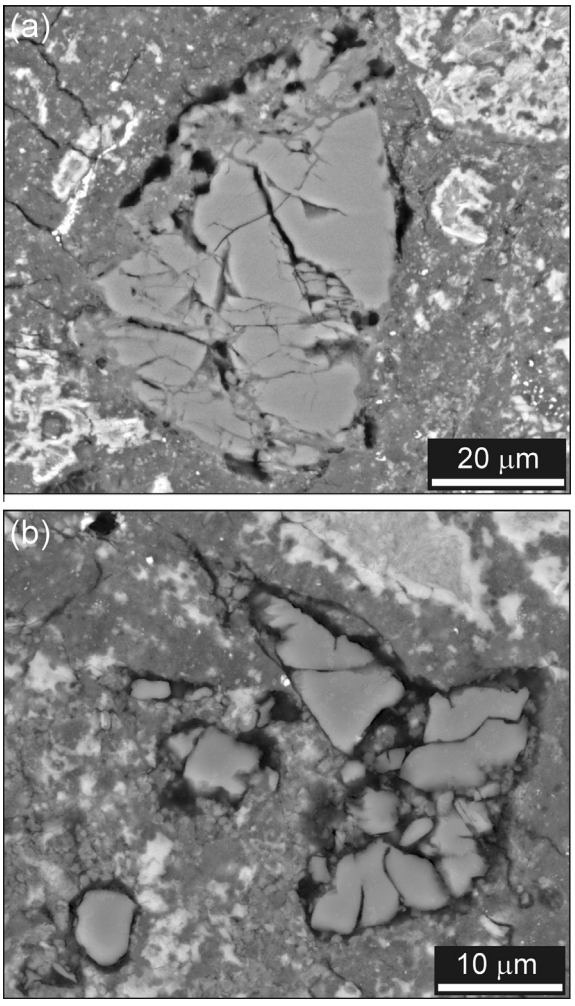

Fig. 2. BSE images of aragonite grains. (a) A grain that is cross-cut by numerous intersecting fractures (black lines). (b) A group of aragonite grains (probably a disaggregated individual) that are rimmed and cross-cut by pores (black areas).

or coarsely polycrystalline, and many of the equant grains are cross-cut by parallel sets of closely spaced narrow pores that are sometimes present in two orientations. The angles between these pores suggest that some lie along $\{10\bar{1}4\}$ cleavages (Fig. 3a) whereas others are more likely to be coincident with $\{\bar{1}018\}$ *e*-twin composition planes (Fig. 3b). Some of the grains display a concentric zoning in SEM-CL images, and the pattern of zoning indicates that they formed by crystals growing towards the center of a pore from its margins. The equant calcite has a mean chemical composition of $Ca_{99.30}Mg_{0.01}Fe_{0.68}CO_3$ ($n = 9$, Table 1) and mean oxygen isotope values of $\delta^{18}O$ $37.5 \pm 0.7‰$, $\Delta^{17}O$ $1.4 \pm 1.1‰$ (1σ) ($n = 7$, Table 2).

All of the equant calcite grains have rims and inclusions of finely crystalline fibrous minerals (Fig. 3a–d) that contain O, Mg, Si, S, Fe and Ni. This habit and composition is consistent with Fe-rich serpentine intergrown with tochilinite (previously termed 'PCP'). The rims are ~1.5 μm in width, and selvages of the same material may cross-cut grains and to divide them into several 'cells' (Fig. 3c). The inclusions occur as fibres less than ~2 μm in length, and ~1.5–2.0 μm diameter radial-fibrous aggregates (Fig. 3b). Where they are more abundant the inclusions merge to make tens of micrometre sized areas that have a ragged interface with calcite (Fig. 3b and c). Intergrown serpentine and tochilinite also occurs in the meteorite matrix as patches that are calcite-free but comparable in size and shape to the equant grains (Fig. 3d and e). The serpentine and tochilinite patches are comparable in chemical composition to 'PCP' from other CM2 carbonaceous chondrites (Table 3).

3.4. Vein calcite

The vein is ~1 mm in length by 0.05–0.25 mm in width and is located to one side of the AEC-poor region (Figs. 1b and 4). Its calcite is inclusion-free, in direct contact with the meteorite matrix (i.e. it lacks the serpentine–tochilinite rims that characterise equant calcite grains) (Fig. 4a), and contains abundant *e*-twins and subgrains (Lindgren et al., 2011). Vein calcite has a mean chemical composition of $Ca_{99.60}Mg_{0.11}Fe_{0.29}CO_3$ ($n = 4$, Table 1) and mean oxygen isotope values of $\delta^{18}O$ $18.4 \pm 0.3‰$, $\Delta^{17}O$ $-0.5 \pm 0.5‰$ (1σ) ($n = 3$, Table 2).

3.5. Micropore-rich calcite

This calcite is characterised by irregular micropores that range from ~1 to 25 μm in diameter, and <~0.2 to ~2.5 μm sized pentlandite inclusions, but it lacks the serpentine–tochilinite rims and inclusions that are typical of equant calcite (Fig. 5). Small grains of micropore-rich calcite occur in the meteorite matrix, where they are intergrown with or rimmed by olivine or pyroxene (Fig. 5a). The largest volumes of micropore-rich calcite occur within chondrules, and the proportion of a chondrule that it occupies varies significantly so that in some of them little or none of the original silicates remain (Fig. 5b). Calcite-bearing chondules are most abundant in the AEC-poor region (Fig. 1b). An X-ray map shows that vein calcite is continuous with micropore-rich calcite in an adjacent chondrule (Fig. 4c) so that calcite in these two contexts must have crystallized at the same time. Owing to the high density of micropores and inclusions, only one reliable chemical analysis of micropore-rich calcite could be obtained (Table 1), and NanoSIMS work was not attempted.

4. DISCUSSION

4.1. Sequence of carbonate mineralisation

LON 94101 contains three generations of Ca-carbonate: aragonite, equant calcite, and vein plus micropore-rich calcite. As cross-cutting relationships between carbonate generations have not been observed, their relative timing of crystallization cannot be determined using petrographic criteria. However, the equant calcite has been partially replaced by serpentine and tochilinite, whereas the vein and micropore-rich calcite has not. This suggests that the equant calcite crystallized prior to the serpentine and tochil-

Table 1
Chemical compositions of LON 94101 Ca-carbonate grains and the calculated Mg/Ca ratios of solutions in equilibrium with them.

	wt%					Mole%					Solution Mg/Ca	
	Ca	Mg	Fe	Sr	Na	$CaCO_3$	$MgCO_3$	$FeCO_3$	$SrCO_3$	Mg/Ca		
Aragonite											$D_{Mg} = 0.0010$	$D_{Mg} = 0.0013$
A1	40.15	bdl	0.32	0.04	0.14	99.39	–	0.56	0.05	–	–	–
A6	39.54	0.01	0.44	0.04	0.14	99.13	0.03	0.79	0.05	0.0003	0.3253	0.2502
A9	39.29	0.04	0.56	0.06	0.15	98.76	0.17	1.01	0.07	0.0017	1.6916	1.3013
A12	39.51	bdl	0.43	0.05	0.12	99.17	–	0.77	0.06	–	–	–
A13	39.65	0.01	0.41	0.08	0.13	99.14	0.04	0.73	0.09	0.0004	0.3909	0.3007
A14	39.02	0.01	0.43	0.08	0.15	99.10	0.03	0.78	0.09	0.0003	0.2916	0.2243
A15	39.22	0.01	0.40	0.07	0.15	99.15	0.04	0.73	0.08	0.0004	0.4078	0.3137
A17	37.90	0.09	0.52	0.08	0.18	98.55	0.38	0.98	0.09	0.0039	3.8767	2.9820
A18	38.74	0.14	0.55	0.04	0.14	98.34	0.60	1.01	0.05	0.0061	6.0878	4.6830
A19	38.86	0.02	0.30	0.05	0.11	99.31	0.08	0.54	0.06	0.0008	0.8105	0.6235
A23	39.77	0.02	0.44	0.06	0.15	99.07	0.07	0.78	0.07	0.0007	0.7257	0.5582
A24	39.64	0.02	0.33	0.07	0.20	99.24	0.09	0.60	0.07	0.0009	0.8820	0.6785
Mean	39.27	0.03	0.43	0.06	0.15	99.03	0.13	0.77	0.07	0.0013	1.2908	0.9929
Equant calcite											$D_{Mg} = 0.04$	$D_{Mg} = 0.01$
E2	39.79	bdl	0.36	bdl	bdl	99.35	–	0.65	–	–	–	–
E3	39.97	bdl	0.37	bdl	0.02	99.34	–	0.66	–	–	–	–
E4	39.77	bdl	0.40	bdl	0.05	99.29	–	0.71	–	–	–	–
E6	39.72	bdl	0.43	bdl	bdl	99.24	–	0.76	–	–	–	–
E7	39.61	bdl	0.37	bdl	bdl	99.33	–	0.67	–	–	–	–
E8	39.35	bdl	0.42	bdl	0.05	99.23	–	0.77	–	–	–	–
E10	39.93	bdl	0.29	bdl	0.05	99.48	–	0.52	–	–	–	–
E12	39.64	bdl	0.40	bdl	0.05	99.28	–	0.72	–	–	–	–
E14	38.96	0.03	0.38	bdl	0.06	99.19	0.12	0.70	–	0.0012	0.0299	0.1198
Mean	39.64	0.00	0.38	0.00	0.03	99.30	0.01	0.68	0.00	0.0001	0.0033	0.0133
Vein and micropore-rich calcite											$D_{Mg} = 0.04$	$D_{Mg} = 0.01$
V1	39.41	0.03	0.12	bdl	0.08	99.65	0.13	0.22	–	0.0013	0.0328	0.1314
V2	39.35	0.03	0.11	bdl	0.08	99.69	0.11	0.21	–	0.0011	0.0267	0.1069
V3	39.05	0.03	0.14	bdl	bdl	99.60	0.14	0.26	–	0.0014	0.0344	0.1377
V4	39.54	0.01	0.27	bdl	0.07	99.45	0.06	0.49	–	0.0006	0.0143	0.0571
M13	39.78	bdl	0.28	bdl	bdl	99.50	–	0.50	–	–	–	–
Mean	39.42	0.02	0.19	0.00	0.05	99.58	0.09	0.34	0.00	0.0009	0.0217	0.0866

Data obtained by EPMA. bdl denotes below detection limits. Mn was below detection limits in all analyses. Na was not included in calculations of mole% carbonate.

inite, and the vein and micropore-rich calcite formed afterwards. By the same reasoning the lack of evidence for replacement of aragonite by serpentine and tochilinite could indicate that aragonite postdated one or both generations of calcite. However, this could also be explained by aragonite being less soluble than calcite during serpentine and tochilinite crystallization. Barber (1981) and Lee and Ellen (2008) suggested that aragonite postdated calcite in the CM2s Murchison and Murray respectively, whereas Sofe (2013) examined intergrowths of the two minerals in Murchison and concluded that aragonite crystallized first. The relative timing suggested by Sofe (2013) would be consistent with Ostwald's rule, which states that where two or more polymorphs of a compound are capable of crystallizing from a supersaturated solution, there is a tendency for the least stable polymorph to crystallize first, followed by polymorphs of greater stability (Threlfall, 2003). At the relatively low *T*s and pressures of a parent body interior during aqueous alteration (<~10 MPa and <~35 °C; Zolensky et al., 1993), calcite is the stable polymorph of $CaCO_3$ (Redfern et al., 1989), and so Ostwald's rule predicts that aragonite is likely to have formed before calcite. Therefore, in the following discussion we assume that the LON 940101 Ca-carbonates formed in the order of: (1) aragonite, (2) equant calcite, (3) vein plus micropore-rich calcite.

4.1.1. Crystallization of aragonite

Aragonite has been recorded from the CM2s Cold Bokkeveld, Cochabamba, Murchison and Murray (Müller et al., 1979; Barber, 1981; Lee and Ellen, 2008), and so LON 94101 is the first aragonite-bearing Antarctic find. As noted above, calcite is the thermodynamically stable polymorph of Ca-carbonate during parent body aqueous alteration, and so the presence of aragonite in LON 94101 and other CM2s is unexpected. However, aragonite forms abiologically from terrestrial seawater, despite calcite again being the stable polymorph. Results of empirical and experimental studies have demonstrated that the polymorph of $CaCO_3$ that crystallizes from solutions of a seawater composition

Table 2
Oxygen isotopic compositions of the three generations of Ca-carbonate in LON 94101.

Analyses	$\delta^{18}O$ (‰)	2σ (‰)	$\delta^{17}O$ (‰)	2σ (‰)	$\Delta^{17}O$ (‰)	2σ (‰)
Aragonite						
A1	39.1	1.2	19.5	1.4	−0.8	1.9
A2	39.6	0.9	21.0	1.4	0.4	1.7
A3	40.3	0.9	19.1	1.4	−1.9	1.7
A6	39.5	1.2	19.7	1.4	−0.9	1.9
A9	40.0	1.2	21.1	1.4	0.3	1.9
A11	40.6	0.9	22.0	1.4	0.9	1.7
Equant calcite						
C1a	37.1	0.7	20.7	2.2	1.4	2.3
C1b	37.7	0.7	19.3	2.2	−0.3	2.3
C3a	38.1	0.7	22.8	2.2	2.9	2.3
C3b	38.4	0.7	22.6	2.2	2.6	2.3
C4a	37.5	0.7	20.5	2.2	1.0	2.3
C4b	37.5	0.7	20.5	2.2	1.0	2.3
C4c	36.4	0.7	19.9	2.2	0.9	2.3
Vein calcite						
C2a	18.7	0.7	8.8	2.2	−0.9	2.3
C2b	18.0	0.7	8.7	2.2	−0.7	2.3
C2c	18.5	0.7	9.6	2.2	0.0	2.3

Data obtained by NanoSIMS and expressed relative to SMOW. Analyses with the suffix a, b and c are from different parts of the same grain.

is controlled principally by their temperature and Mg/Ca ratio (Hardie, 1996; Morse et al., 1997; Balthasar et al., 2011). These findings predict that at the temperatures of CM2 aqueous alteration (~20–35 °C; Guo and Eiler, 2007), aragonite will form in preference to calcite where solution Mg/Ca is >~0.5–1.0. Experiments using sulphate-free solutions at 21 °C have found that aragonite is the dominant of the two polymorphs where Mg/Ca is greater than ~0.6–0.7, and the only carbonate to crystallize where Mg/Ca is >~1.7 (Bots et al., 2011).

The possibility that Mg/Ca ratio controlled the polymorph of Ca-carbonate that crystallized in parent body interiors can be tested by determining the Mg/Ca ratio of solutions that would have been in equilibrium with the three LON 94101 Ca-carbonate generations. The experimentally determined partition coefficients of Mg (D_{Mg}) into aragonite and calcite are both temperature dependent, and so here we have used values over the range of 25–35 °C. At these temperatures D_{Mg} for aragonite ranges from 0.0013 to 0.0010 (Gaetani and Cohen, 2006) and D_{Mg} for calcite from ~0.01 to 0.04 (Huang and Fairchild, 2001). The molar Mg/Ca ratios of LON 94101 aragonite, equant calcite, and vein and micropore-rich calcite are listed in Table 1 along with the estimated molar Mg/Ca values for parent body solutions in equilibrium with each carbonate generation. Thus, solutions in equilibrium with aragonite had a molar Mg/Ca ratio of ~1.0–1.3 whereas those in equilibrium with the two calcite generations had Mg/Ca values an order of magnitude lower (Table 1). These results are consistent with Mg/Ca strongly influencing the mineralogy of Ca-carbonate that formed in LON 94101, despite the chemical composition, Eh and pH of parent body fluids (e.g. Zolensky et al., 1993; Riciputi et al., 1994; Guo and Eiler, 2007) being very different to the seawater solutions used in previous studies of Ca-carbonate polymorphism.

If aragonite predated both generations of calcite, solution Mg/Ca must have fallen abruptly after it had formed and remained low. However, in a chemically closed system and without any other competing reactions, the precipitation of Mg-poor Ca-carbonates will raise solution Mg/Ca. Thus, another reaction must have removed Mg from solution in preference to Ca after aragonite had crystallized, and the most likely one is the precipitation of Mg-serpentine, $Mg_3Si_2O_5(OH)_4$, which is abundant in the meteorite matrix (e.g. Barber, 1981).

4.1.2. Precipitation and replacement of equant calcite

Equant grains of calcite are a ubiquitous albeit volumetrically minor constituent of the CM2 meteorites (e.g. Fuchs et al., 1973; Brearley, 1998; Benedix et al., 2003; Lee and Ellen, 2008; de Leuw et al., 2010; Tyra et al., 2012). The Ca for calcite (and aragonite) may have been derived from chondrule mesostases (Brearley, 2006), and this suggestion is supported by the observation that mesostases in the least altered CM2s, for example QUE 97990 (CM2.6; Rubin et al., 2007), retain Ca-silicates including diopside (Maeda et al., 2009). CO_2 for the Ca-carbonates was most likely derived from oxidation of organic matter, and from accreted CO_2, CH_4, CH_3OH ices (Alexander et al., 2013). The SEM-CL zoning of some grains indicates that the trace element concentrations of ambient solutions varied during crystal growth, although the identity of cathodoluminescence the activator(s) in carbonaceous chondrite calcite remains to be determined (Lee and Ellen, 2008). Those grains that are apparently unzoned are interpreted to have grown more rapidly than the rate of change in solution chemistry.

Equant calcite grains in many CM2s in addition to LON 94101 have a narrow rim of serpentine and tochilinite (Browning and Bourcier, 1998; Lee and Ellen, 2008; de

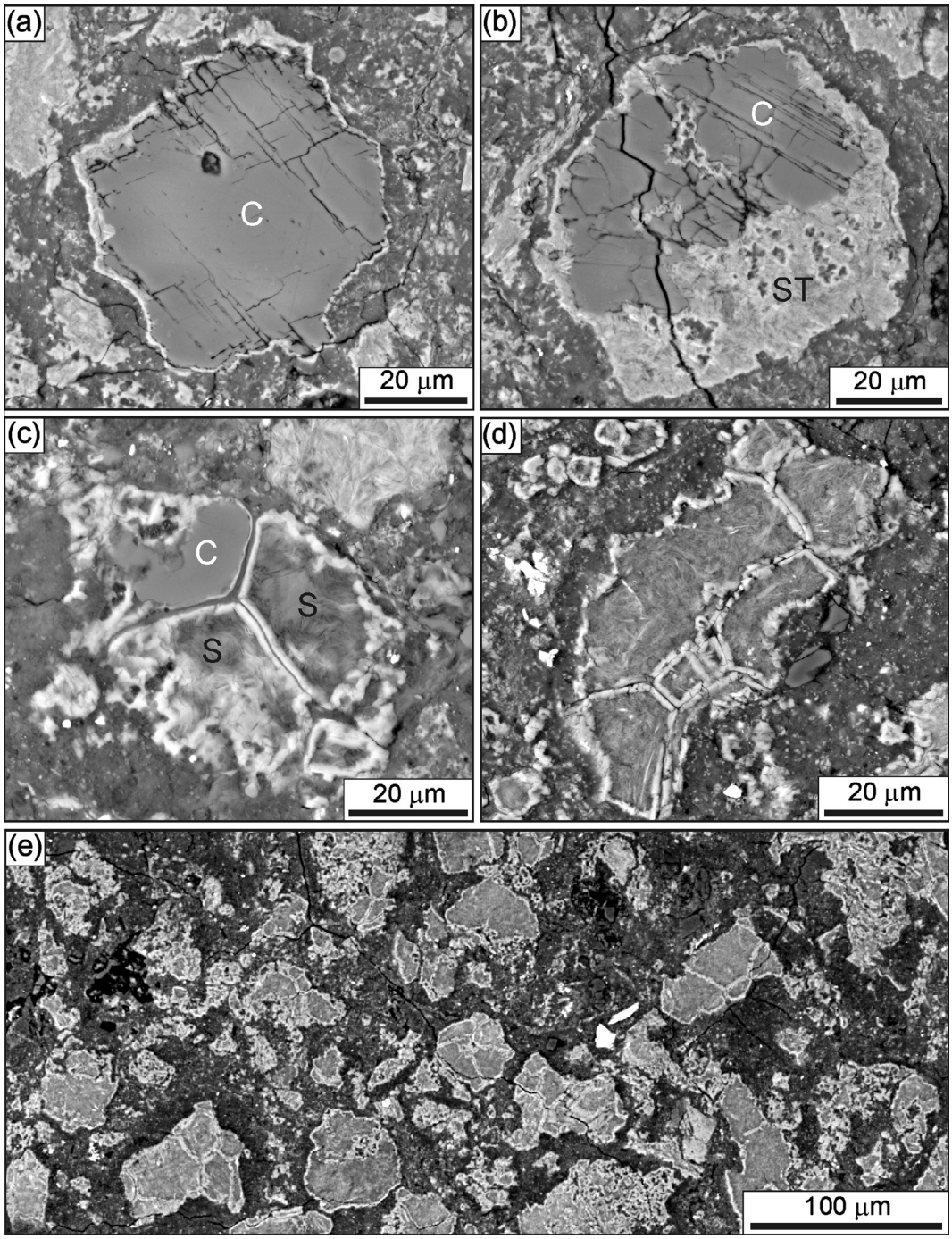

Fig. 3. BSE images of equant calcite (C) grains and associated serpentine and tochilinite. (a) A calcite grain with a narrow serpentine–tochilinite rim (white). The grain is cross-cut by linear pores whose angles of intersection indicate that have formed along $\{10\bar{1}4\}$ cleavage planes. (b) A calcite grain that has been partially replaced by intergrown serpentine and tochilinite (ST) on its lower right hand side. Closely spaced pairs of narrow pores in the calcite have probably formed along the composition planes of $\{\bar{1}018\}$ *e*-twins. (c) An object that is divided into three 'cells' by serpentine–tochilinite selvages (white). Two of the cells contain serpentine (S) whereas the third hosts calcite. (d) A patch of serpentine and tochilinite that has a faceted outline and a cellular internal structure but lacks calcite. (e) Serpentine–tochilinite patches (white and light grey) enclosed by meteorite matrix (dark grey) in the AEC-poor region. The serpentine–tochilinite patches occupy 22 vol.% of this field of view.

Leuw et al., 2010). Petrographic relationships between these minerals suggest that serpentine and tochilinite rims and inclusions formed by replacement of calcite (Fig. 3a–c). An alternative explanation for these intergrowths is that calcite has partially replaced patches of serpentine and tochilinite. However, this possibility is considered unlikely because the pattern of SEM-CL zoning is consistent with formation of equant grains by cementation of fluid-filled

Table 3
Chemical compositions of LON 94101 serpentine–tochilinite patches compared with 'PCP'.

wt%	P1	P2	P7	P11	P13	'PCP'
SiO_2	17.73	17.01	16.79	30.23	28.61	20.3
TiO_2	0.04	0.04	0.04	0.04	0.05	0.07
Al_2O_3	2.57	2.17	2.35	1.97	1.65	2.5
Cr_2O_3	0.13	0.16	0.23	0.21	0.28	0.29
FeO	36.62	35.67	40.37	21.50	21.96	36.7
MnO	0.23	0.20	0.14	0.18	0.24	0.19
NiO	3.31	3.01	2.37	1.35	2.06	1.70
MgO	14.90	14.44	12.01	24.18	24.08	13.5
CaO	0.20	0.12	0.14	0.10	0.13	0.41
Na_2O	0.31	0.26	0.40	0.34	0.23	0.18
K_2O	0.06	0.04	0.06	0.12	0.08	0.04
S	8.39	8.24	8.02	3.23	5.49	4.10
Total	84.49	81.36	82.92	83.45	84.86	79.98

Data obtained by EPMA, and expressed in wt%. P was below detection limits in all analyses. P1–P13 are individual analyses of LON 94101 serpentine–tochilinite patches, and 'PCP' is serpentine–tochilinite in QUE 99355 (CM2.3; Rubin et al. 2007), which has a comparable degree of aqueous alteration to LON 94101.

pores, and it is difficult to account for why calcite would commonly stop short of completely replacing the serpentine and tochilinite to leave a thin rim remaining (e.g. Fig. 3a).

Many of the patches of serpentine and tochilinite lack calcite inclusions (Fig. 3d and e). Some of these patches, and in particular those with angular outlines and cell-like internal divisions (Fig. 3d), are interpreted to be pseudomorphs of equant calcite grains. As the abundance of angular serpentine-tochilinite patches can attain tens of vol.% (Fig. 3e), a significant quantity of equant calcite may have been lost from LON 94101 by replacement. Browning and Bourcier (1998) proposed the following reaction for replacement of calcite by serpentine and tochilinite:

$$CaCO_3 + 0.69Fe^{2+} + 0.38HS^- + 0.63H_2O \rightarrow Ca^{2+} + HCO_3^- + 0.63\text{Tochilinite} \quad (1)$$

$$CaCO_3 + 0.01SiO_{2(aq)} + 0.5Fe^{2+} + 0.75H_2O + 0.06O_{2(aq)} \rightarrow Ca^{2+} + HCO_3^- + 0.13\text{Cronstedtite} \quad (2)$$

These reactions will enrich aqueous solutions in Ca and HCO_3^-, which may have contributed to formation of the second calcite generation in LON 94101, as discussed below. Models of the aqueous alteration of CM2 carbonaceous chondrites suggest that Fe-rich serpentine and tochilinite would have formed early and following the liberation of S, Si and Fe from sulphides and Fa-rich olivine (Tomeoka and Buseck, 1985). As these minerals postdate equant calcite (and so also aragonite), the first two generations of LON 94101 Ca-carbonate must have formed during even earlier stages of water–rock interaction.

4.1.3. Vein and micropore-rich calcite

The petrographic relationships between vein and micropore-rich calcite show that they formed during the same episode of Ca-carbonate mineralisation (Fig. 4c). A genetic link is also supported by the occurrence of the vein on the edge of the AEC-poor region, within which calcite-bearing chondrules are abundant (Fig. 1b and c). As vein calcite is free of matrix inclusions, it is interpreted to have formed

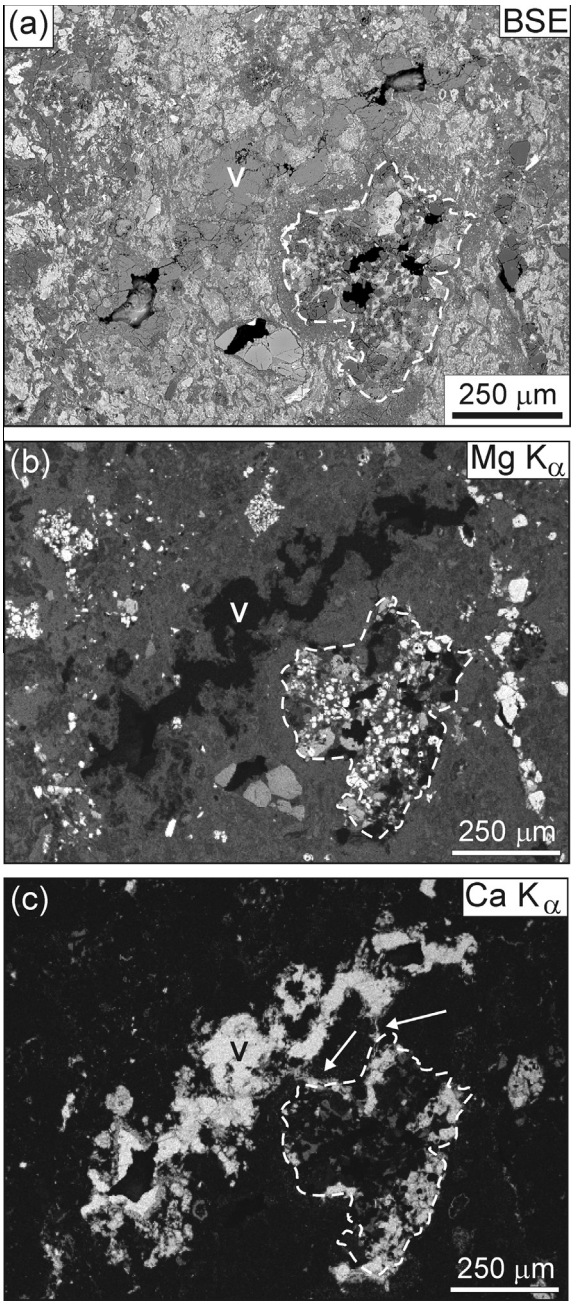

Fig. 4. BSE image (a) and X-ray maps (b) and (c) of the area on the edge of the AEC-poor region that contains the calcite vein (V). The vein is oriented NE-SW, and just beneath it is a chondrule that has been partially replaced by calcite, and whose edges are delineated by a dashed white line. In the Mg K_α map (b) grains of olivine/pyroxene are white, matrix and mesostasis phyllosilicates are mid-grey and vein (V) and chondrule calcite is black. The map demonstrates that the chondrule has been only partially altered so that it retains some of its original anhydrous silicates. The Ca K_α X-ray map (c) shows that vein calcite (white) is connected to chondrule calcite by two narrow veins (arrowed).

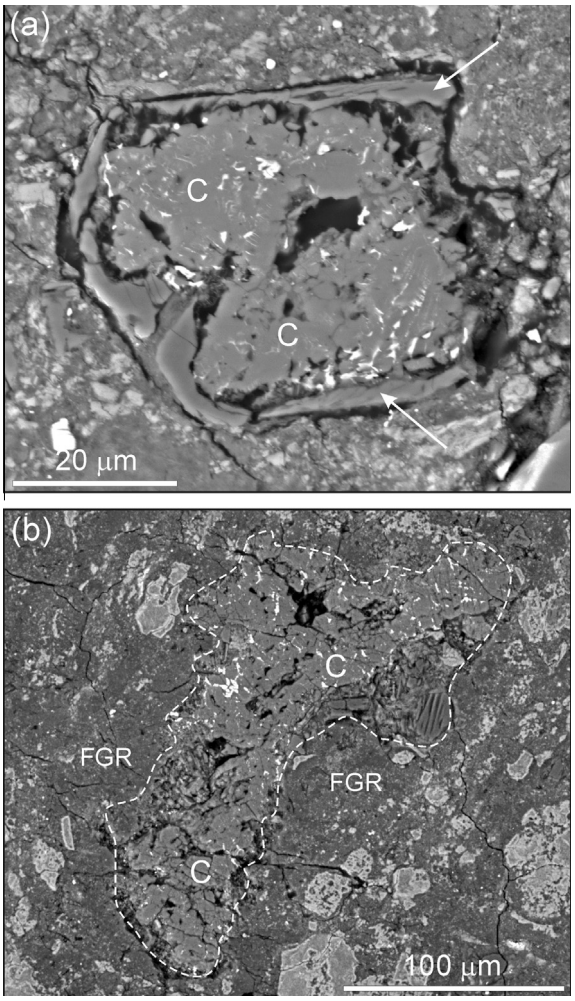

Fig. 5. BSE images of micropore-rich calcite (C). (a) An anhydrous silicate grain in the meteorite matrix that has been partially replaced by calcite. The calcite contains irregular micropores (black) and inclusions of pentlandite (white). Only the rim of the original silicate grain remains (arrowed). (b) A former chondrule fragment (whose edges are delineated by a dashed white line) that has been completely replaced by micropore-rich calcite. Its fine-grained rim (FGR) has been unaffected.

by cementation of a fluid-filled fracture (Lindgren et al., 2011). By contrast, the intergrowth of micropore-rich calcite with anhydrous ferromagnesian silicates is consistent with a replacive origin, and the micropores that characterise this calcite are typical of the products of dissolution-reprecipitation reactions in a wide variety of mineral systems (Putnis, 2002; Parsons and Lee, 2009). Micropore-rich calcite containing micrometre-sized inclusions of pentlandite has also been interpreted to have formed by replacement of chondrules in the CM2 meteorites Cold Bokkeveld (Lee, 1993), ALH 81002 (Hanowski and Brearley, 2001), and EET 96006-paired (the 'Type 2' calcite of Tyra et al., 2012).

The replacement of anhydrous silicates by calcite is termed carbonation, and this reaction has been studied extensively with regards to developing strategies for the long-term storage of terrestrial CO_2 (e.g. Matter and Kelemen, 2009; Kelemen et al., 2011). Carbonation of CM2 chondrules might be expected to yield a Mg- and Fe-bearing carbonate given that it has replaced ferromagnesian silicates, yet the micropore-rich calcite is compositionally near-pure (i.e. $Ca_{99.5}Fe_{0.5}CO_3$; Table 1). This contradiction was also noted in an experimental study of olivine carbonation by Hövelmann et al. (2011), and they concluded that the crystallization of magnesite ($MgCO_3$) had been kinetically inhibited relative to calcite owing to the hydration of Mg^{2+} ions. In these experiments carbonic acid (H_2CO_3) reacted with olivine to consume protons, and as bicarbonate activity increased the Ca-rich fluid at the dissolving olivine surface became supersaturated with respect to calcite (Eq. (3), modified from Hövelmann et al., 2011).

$$Mg_xFe_{2-x}SiO_4 + Ca^{2+} + H_2CO_3 + 2H \rightarrow CaCO_3 + SiO_2 + xMg^{2+} + 2 - xFe^{2+} + 2H_2O \quad (3)$$

This reaction requires a sink for Mg, Fe and SiO_2. The presence of pentlandite within the micropore-rich calcite suggests that a proportion of the Fe liberated during replacement combined with S that was also in solution (not included in Eq. (3)) to precipitate the sulphide. Alternatively both the S and Fe may have been derived from opaque inclusions. Mg must have been exported from the reaction site along with Si, and these elements could then have been available for crystallization of other minerals elsewhere in the meteorite.

Carbonation of the LON 94101 ferromagnesian silicates requires introduction of CO_2 and some or all of the Ca required to form calcite. It is likely that by the time of vein and micropore-rich calcite formation the most soluble Ca-rich silicates (e.g. chondrule mesostases) had been aqueously altered. Ca could have been derived locally from a non-silicate source, or introduced from another parent body region. A suitable local source of Ca would have been the congruent dissolution of aragonite and replacement of equant calcite (e.g. Eqs. (1) and (2)), and this hypothesis is consistent with the scarcity of both generations of Ca-carbonate in the AEC-poor region of the thin section, which contains the vein and calcitized chondrules (Fig. 1b and c). Dissolution and replacement of aragonite and equant calcite, and later reprecipitation of micropore-rich calcite, may have been focused in one part of LON 94101 because the fracture (which was subsequently mineralised to form the vein) served as a reservoir or conduit for aqueous solutions. In this scenario, LON 94101 must have been fractured after the formation of aragonite and equant calcite, but before completion of serpentine and tochilinite precipitation. In common with Ca, much of the CO_2 required for carbonation could have been sourced locally by dissolution and replacement of aragonite and equant calcite (e.g. Eqs. (1) and (2)). The other possibility is that Ca and CO_2 were introduced into LON 94101 via fluid sourced from another part of the parent body, and the vein may be a vestige of the conduit. Oxygen isotopic data may provide further insight into the provenance of solutions from which the three Ca-carbonate generations crystallized.

4.2. Oxygen isotopic evolution of parent body solutions

The bulk oxygen isotopic composition of Ca-carbonates in the CM2 meteorites has been reported by Grady et al. (1988; $\delta^{18}O$ and $\delta^{13}C$), Clayton and Mayeda (1984; $\delta^{17}O$ and $\delta^{18}O$), Benedix et al. (2003; $\delta^{17}O$ and $\delta^{18}O$), Guo and Eiler (2007; $\delta^{18}O$ and $\delta^{13}C$) and Tyra et al. (2007; $\delta^{17}O$ and $\delta^{18}O$). Ion microprobe analyses of $\delta^{17}O$ and $\delta^{18}O$ within individual grains from single meteorites have been described by Brearley et al. (1999; Murchison), Bonal et al. (2010; Murchison), Tyra et al. (2012; EET 96006-paired) and Jenniskens et al. (2012; Sutter's Mill). The bulk analyses yield data with a high precision but will average the compositions of isotopically distinct generations of Ca-carbonate if present, whereas the ion microprobe analyses can be targeted to preselected generations of grains, or even parts of a single grain, but are less precise. Here we present the first analyses of the oxygen isotope composition of aragonite in any meteorite, although as this mineral occurs in many CM2s, albeit in low abundance (Sofe et al., 2011), oxygen isotope analyses of bulk samples will have contained contributions from both of the Ca-carbonate polymorphs. It is also possible that a proportion of the Ca-carbonate grains that were analysed in previous ion microprobe studies were aragonite rather than calcite because techniques to distinguish the two polymorphs were not used in some of those studies. Before discussing the LON 94101 data (Fig. 6), existing models of the oxygen isotope evolution of parent body fluids are reviewed.

Results from the previous three-isotope ion microprobe studies show that the populations of Ca-carbonate grains within individual CMs have a range of $\delta^{18}O$ values and the array lies close and near-parallel to the slope 0.52 TFL on a plot of $\delta^{17}O$ against $\delta^{18}O$ (Fig. 7). The bulk oxygen isotope values of Ca-carbonate in different CM meteorites also has a significant range and again defines a trend line near to the TFL (Benedix et al., 2003) (Fig. 7). This correspondence between bulk and grain-scale oxygen isotope values implies that each CM2 contains a population of Ca-carbonate grains that has a different range of $\delta^{17}O$ and $\delta^{18}O$ values. The spread of Ca-carbonate oxygen isotope values within each CM2 can be interpreted in several ways. It may reflect precipitation at different times from a solution whose oxygen isotope composition was evolving in response to mixing between two reservoirs with distinct oxygen isotope values, namely water derived from the melting of accreted H_2O ices (^{16}O-depleted) and primary anhydrous silicate minerals (^{16}O-enriched) (Benedix et al., 2003). The initial water may have had a value of $\delta^{17}O$ 17.7‰, $\delta^{18}O$ 28.1‰ (i.e. $\Delta^{17}O = 3.09$) whereas the primary silicates could have a value of $\delta^{17}O$ −7.4‰, $\delta^{18}O$ −4.2‰ (i.e. $\Delta^{17}O = -5.22$) (Clayton and Mayeda, 1984, 1999). Owing to the fall in $\Delta^{17}O$ values during progressive water–rock interaction, the mixing line between the two end members has a slope of >0.52 on a plot of $\delta^{17}O$ against $\delta^{18}O$. The array of oxygen isotope values of Ca-carbonate grains could also be interpreted to indicate that they crystallized from solutions that were flowing along a temperature gradient (e.g. Young et al., 1999). In this case the array should have a slope of ~0.52 in a three-isotope plot, but the model of Young et al. (1999) predicts that Ca-carbonate $\delta^{17}O$ and $\delta^{18}O$ values should in general increase as alteration progresses. Thus, an understanding of the relative chronology of Ca-carbonate mineralisation in LON 94101 is important for interpreting the driver(s) of the observed changes in oxygen isotope values.

4.2.1. Aragonite and the switch to equant calcite

The aragonite analyses are indistinguishable within error with respect to their $\delta^{18}O$ and $\Delta^{17}O$ values (Table 2, Fig. 6), which suggests that the grains analysed grew in equilibrium with solutions of essentially the same oxygen isotopic composition and temperature. Aragonite and equant calcite are indistinguishable in $\Delta^{17}O$, but their mean $\delta^{18}O$ values differ, i.e. $\delta^{18}O$ of 39.9 ± 0.6‰ (1σ) *vs* 37.5 ± 0.7‰ (1σ) respectively (Fig. 6). This difference in $\delta^{18}O$ may be largely due to contrasting fractionation factors of the two minerals. If they had crystallized in equilibrium with a solution of the same oxygen isotopic value and temperature, aragonite would have been enriched in ^{18}O relative to calcite by ~0.8‰ (Kim et al., 2007). Thus although the aragonite and equant calcite are likely to have precipitated from a solution whose oxygen isotopic composition and temperature had remained relatively unchanged, its Mg/Ca ratio had fallen in response to withdrawal of Mg from solution in preference to Ca, for example by crystallization of Mg-serpentine.

4.2.2. Equant, vein and micropore-rich calcite

The equant calcite analyses are indistinguishable with regards to $\Delta^{17}O$, but there is an intergranular difference in $\delta^{18}O$ values (Fig. 6), which points towards a small spatial or temporal variation in solution $\delta^{18}O$ or temperature during mineralisation. The magnitude of the difference in $\delta^{17}O$ and $\delta^{18}O$ between the equant and vein calcite (Fig. 6) indicates that the two generations crystallized in discrete events. Their mean $\Delta^{17}O$ values are distinct (1.4 ± 1.1‰ *vs* -0.5 ± 0.5‰), which would be consistent with the vein and micropore-rich calcite having grown in equilibrium with solutions that had become enriched in ^{16}O by interaction with anhydrous silicates (i.e. consistent with the closed

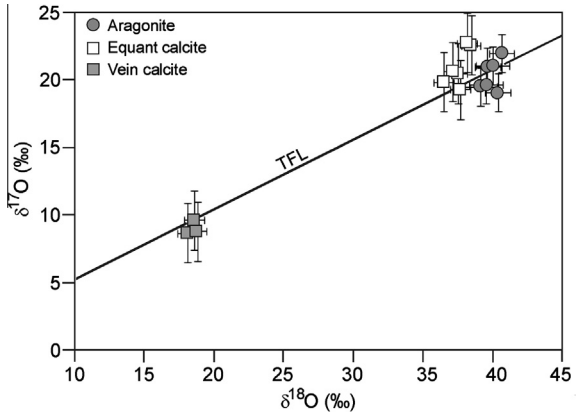

Fig. 6. Plot of $\delta^{17}O$ *vs* $\delta^{18}O$ (both relative to SMOW) for the three Ca-carbonate generations in LON 94101. The error bars are 2σ. TFL denotes the terrestrial fractionation line.

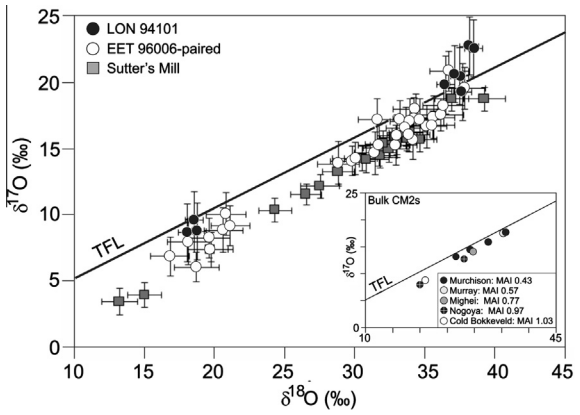

Fig. 7. Plot of $\delta^{17}O$ *vs* $\delta^{18}O$ (both relative to SMOW) for calcite in EET 96006-paired (Tyra et al., 2012; 1σ errors), Sutter's Mill (Jenniskens et al., 2012; 2σ errors) and LON 94101 (this study; 2σ errors). The equations of trend lines regressed through the datasets are: LON 94101 $\delta^{17}O = 0.62$ (±0.03, 1σ)·$\delta^{18}O$ −2.46 (±1.1, 1σ); EET 96006-paired $\delta^{17}O = 0.61$ (±0.02, 1σ)·$\delta^{18}O$ −3.67 (±0.7, 1σ); Sutter's Mill $\delta^{17}O = 0.62$ (±0.01, 1σ)·$\delta^{18}O$ −4.80 (±0.4, 1σ). The inset shows $\delta^{17}O$ *vs* $\delta^{18}O$ for bulk CM2 carbonate analyses (25 °C extraction) in Benedix et al. (2003) (error bars are smaller than the datapoints). The Mineral Alteration Index (MAI) of each meteorite is stated, whereby the higher value represents a greater degree of alteration. TFL denotes the terrestrial fractionation line.

system two-reservoir model). A proportion of the difference in the oxygen isotopic compositions of the two generations of calcite could also be due to a contrast in fluid temperature. However, in order to account for all of the change in $\delta^{18}O$ between equant and vein calcite (i.e. a fall from a mean of 37.5 ± 0.7‰ to 18.4 ± 0.3‰) the solutions in equilibrium with vein calcite would need to have been substantially hotter. As the oxygen isotope composition of parent body solutions in equilibrium with equant and vein calcite are unknown, their temperatures cannot be determined. Therefore, the LON 94101 calcite oxygen isotope data do not definitively identify the processes by which fluids evolved between crystallization of equant and vein plus micropore-rich calcite. The various possibilities may be evaluated further by comparison with conclusions from the previous three-isotope studies.

From determinations of the bulk oxygen isotopic composition of calcite in the CM2s Murchison, Murray, Mighei, Nogoya and Cold Bokkeveld, Benedix et al. (2003) demonstrated an inverse correlation between the meteorite's degree of aqueous alteration (as quantified using the Mineral Alteration Index, MAI), and $\Delta^{17}O$ (i.e. the more highly altered CM2s had a lower $\Delta^{17}O$ value; Fig. 7). Although these results were consistent with two-component mixing within static fluids Clayton and Mayeda (1984, 1999), Benedix et al. (2003) showed that the fluid flow model of Young et al. (1999) described a region within a planetesimal that shared the relationship that they had observed between $\Delta^{17}O$ and degree of alteration. Tyra et al. (2012) described two generations of calcite in EET 96006-paired that have similar $\delta^{17}O$ and $\delta^{18}O$ values to the generations in LON 94101 (Fig. 7). Their Type 1 calcite is petrographically equivalent to the LON 94101 equant calcite grains whereas the EET 96006-paired Type 2 calcite has replaced chondrules, and so is petrographically comparable to the

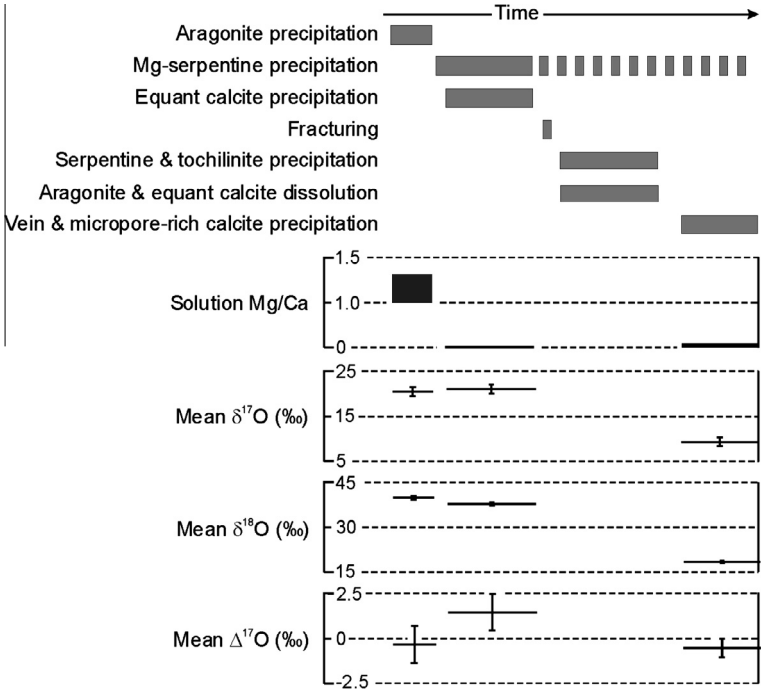

Fig. 8. Summary of the sequence of Ca-carbonate mineralisation and associated events in LON 94101. Also shown are the calculated ranges of Mg/Ca ratios of aqueous solutions in equilibrium with aragonite and calcite, and the mean oxygen isotopic compositions of each Ca-carbonate generation (relative to SMOW, with 1σ error bars).

LON 94101 micropore-rich calcite. Drawing on the two-component mixing interpretation of the whole rock carbonate results in Benedix et al. (2003), Tyra et al. (2012) concluded that their Type 1 calcite had formed first and in equilibrium with aqueous solutions that had undergone less interaction with primary anhydrous silicates than the more evolved solutions from which the Type 2 calcite precipitated. Jenniskens et al. (2012) showed that calcite in Sutter's Mill (CM2.0/CM2.1) has a greater range in $\delta^{17}O$ and $\delta^{18}O$ values than recorded by Tyra et al. (2012), and although two populations may be present, the division between them is less distinct than for LON 94101 or EET 96006-paired (Fig. 7). Jenniskens et al. (2012) and Kohl et al. (2013) concluded that the solutions from which Sutter's Mill carbonates crystallized had flowed along a temperature gradient so that the grains differ in $\delta^{17}O$ and $\delta^{18}O$, but $\Delta^{17}O$ values are largely invariant. Whilst this model could also account for the LON 94101 data, Young et al. (1999) predicted that the solutions would evolve towards higher $\delta^{17}O$ and $\delta^{18}O$ values, yet in LON 94101 the petrographic evidence shows that isotopic evolution was towards a lower $\delta^{17}O$ and $\delta^{18}O$.

The LON 94101 oxygen isotopic data therefore demonstrate that between crystallization of the two calcite generations there was a fall in fluid $\Delta^{17}O$, together with a change in $\delta^{17}O$ and $\delta^{18}O$ and/or temperature. This isotopic evolution is broadly consistent with the two-component mixing model, but the question of the provenance of the solutions remains unanswered. The fluids from which the carbonates formed could have changed chemically, isotopically and thermally *in situ*, or the vein and micropore-rich calcite may have crystallized from isotopically more evolved and/or hotter fluids that were introduced into LON 94101 from another region of the parent body. The latter possibility is here considered more likely because the mineralised fracture is located on the edge of an area of LON 94101 that is depleted in equant calcite and aragonite, and contains the largest calcitized chondrules. Thus, after crystallization of aragonite and equant calcite we suggest that fractures developed, which enabled a new pulse of solutions to enter LON 94101 (Fig. 8). These fluids locally enhanced the ongoing replacement of equant calcite by serpentine and tochilinite (to make the AEC poor region), and mediated crystallization of the second calcite generation. Although the region of the parent body from where LON 94101 was derived had a locally high permeability along fractures, the matrix permeability was probably very low (Bland et al., 2009), so that once the new solutions entered LON 94101 they remained localised. This model is consistent with suggestions by Tyra et al. (2012) and Rubin (2012) that episodic parent body aqueous activity may have been impact-related, and the mineralised fracture confirms that LON 94101 experienced extensional stress prior to formation of the second calcite generation. Tyra et al. (2012) suggested that the Type 2 calcite in EET 96006-paired could have crystallized in response to the degassing of CO_2 from solution following a sudden pressure release, and the same process could also account for the formation of vein and micropore-rich calcite in LON 94101.

5. CONCLUSIONS

Ca-carbonate minerals in LON 94101 provide three snapshots of the evolution of parent body aqueous solutions (Fig. 8). Grains of aragonite and equant calcite formed first by cementation of tens of micrometre-sized pores. They crystallized in equilibrium with solutions of a similar oxygen isotopic composition and temperature, although different Mg/Ca ratio (Fig. 8). Therefore these two Ca-carbonate minerals are likely to have formed over a short time period early in the aqueous alteration history of LON 94101 whilst fluids were evolving in response to precipitation of minerals including Mg-serpentine. Subsequently a new pulse of solutions with lower $\Delta^{17}O$, $\delta^{17}O$ and $\delta^{18}O$ values, and possibly also a higher temperature, entered LON 94101 via a fracture network. These solutions mediated the congruent and incongruent dissolution of aragonite and equant calcite, and then crystallization of calcite within an open fracture (to form the calcite vein) and by replacement (i.e. carbonation) of silicate minerals (Fig. 8).

Isotopically distinct generations of calcite have been described from EET 96006-paired, Sutter's Mill and LON 94101 (Fig. 7), supporting the prediction by Tyra et al. (2012) that multiphase carbonates are commonplace in the CM2 carbonaceous chondrites. Both EET 96006-paired and LON 94101 contain two generations of calcite that differ significantly in $\delta^{17}O$ and $\delta^{18}O$, and we suggest that the second and isotopically lighter generation of calcite could have formed in response to an event such as an impact that mobilised aqueous solutions throughout a substantial (tens of metre sized or more) region of a common parent body. This hypothesis needs to be tested by further integrated petrographic, mineralogical and isotopic studies of CM2s, but results of this study nonetheless demonstrate that their Ca-carbonates can provide new and valuable insights into the internal structure and evolution of parent bodies.

ACKNOWLEDGEMENTS

We are grateful to the NASA Antarctic meteorite collection for loan of the LON 94101 thin section, Peter Chung for help with the SEM work, Chris Hayward for assistance with EPMA analyses, and Nick Kamenos for statistical advice. NanoSIMS access through UKCAN is gratefully acknowledged, and we thank STFC for supporting this research. Careful and knowledgeable reviews from Kazushige Tomeoka and Mark Tyra substantially improved this manuscript.

REFERENCES

Alexander C. M. O'D., Bowden R., Fogel M. L. and Howard K. T. (2013) Carbonate abundances and isotopic compositions in chondrites. *Lunar Planet. Sci. 44*. Lunar Planet. Inst., Houston. #2788 (abstr.).

Antarctic Meteorite Newsletter (1995) vol. 18, no. 2. JSC, NASA Johnson Space Center, Houston, TX (August).

Balthasar U., Cusack M., Faryma L., Chung P., Holmer L. E., Percival I. G. and Popov L. E. (2011) Relic aragonite from Ordovician–Silurian brachiopods – implications for evolution of calcification. *Geology* **39**, 967970.

Barber D. J. (1981) Matrix phyllosilicates and associated minerals in C2M carbonaceous chondrites. *Geochim. Cosmochim. Acta* **45**, 945970.

Benedix G. K., Leshin L. A., Farquhar J., Jackson T. and Thiemens M. H. (2003) Carbonates in CM2 chondrites: Constraints on alteration conditions from oxygen isotopic compositions and petrographic observations. *Geochim. Cosmochim. Acta* **67**, 15771588.

Bland P. A., Jackson M. D., Coker R. F., Cohen B. A., Webber B. W., Lee M. R., Duffy C. M., Chater R. J., Ardakani M. G., McPhail D. S., McComb D. W. and Benedix G. K. (2009) Why aqueous alteration in asteroids was isochemical: High porosity ≠ high permeability. *Earth Planet. Sci. Lett.* **287**, 559–568.

Bonal L., Huss G. R., Krot A. N. and Nagashima K. (2010) Chondritic lithic clasts in the CB/CH-like meteorite Isheyevo: Fragments of previously unsampled parent bodies. *Geochim. Cosmochim. Acta* **74**, 25002522.

Bots P., Benning L. G., Rickaby R. E. M. and Shaw S. (2011) The role of SO_4 in the switch from calcite to aragonite seas. *Geology* **39**, 331–334.

Brearley A. J. (1998) Carbonates in CM carbonaceous chondrites: Complex zoning revealed by high resolution cathodoluminescence studies. *Lunar Planet. Sci. 29*. Lunar Planet. Inst., Houston. #1246 (abstr.).

Brearley A. J. (2006) The role of microchemical environments in the alteration of CM carbonaceous chondrites. *Lunar Planet. Sci. 37*. Lunar Planet. Inst., Houston. #2074 (abstr.).

Brearley A. J. and Hutcheon I. D. (2000) Carbonates in the CM1 chondrite ALH 84034: Mineral chemistry, zoning and Mn–Cr systematics. *Lunar Planet. Sci. 31*. Lunar Planet. Inst., Houston. #1407 (abstr.).

Brearley A. J. and Hutcheon I. D. (2002) Carbonates in the Y791198 CM2 chondrite: Zoning and Mn–Cr systematics (abstract). *Meteorit. Planet. Sci.* **37**, A23.

Brearley A. J., Saxton J. M., Lyon I. C. and Turner G. (1999) Carbonates in the Murchison CM chondrite: CL characteristics and oxygen isotopic compositions. *Lunar Planet. Sci. 30*. Lunar Planet. Inst., Houston. #1301 (abstr.).

Brearley A. J., Hutcheon I. D. and Browning L. (2001) Compositional zoning and Mn–Cr systematics in carbonates from the Y791198 CM2 carbonaceous chondrite. *Lunar Planet. Sci. 32*. Lunar Planet. Inst., Houston. #1458 (abstr.).

Browning L. B. and Bourcier W. L. (1998) On the origin of rim textures surrounding carbonate grains in CM matrices. *Lunar Planet. Sci. 29*. Lunar Planet. Inst., Houston. #1533 (abstr.).

Clayton R. N. and Mayeda T. K. (1984) The oxygen isotope record in Murchison and other carbonaceous chondrites. *Earth Planet. Sci. Lett.* **67**, 151–161.

Clayton R. N. and Mayeda T. K. (1999) Oxygen isotope studies of carbonaceous chondrites. *Geochim. Cosmochim. Acta* **63**, 2089–2104.

de Leuw S., Rubin A. E., Schmidt A. K. and Wasson J. T. (2009) ^{53}Mn–^{53}Cr systematics of carbonates in CM chondrites: Implications for the timing and duration of aqueous alteration. *Geochim. Cosmochim. Acta* **73**, 7433–7442.

de Leuw S., Rubin A. E., Schmidt A. K. and Wasson J. T. (2010) Carbonates in CM chondrites: Complex formational histories and comparison to carbonates in CI chondrites. *Meteorit. Planet. Sci.* **45**, 513–530.

DuFresne E. R. and Anders E. (1962) On the chemical evolution of the carbonaceous chondrites. *Geochim. Cosmochim. Acta* **26**, 1085–1114.

Fuchs L. H., Olsen E. and Jensen K. J. (1973) Mineralogy, mineral chemistry and composition of the Murchison (C2) meteorite. *Smithson. Contrib. Earth Sci.* **10**, 139.

Fujiya W., Sugiura N., Hotta H., Ichimura K. and Sano Y. (2012) Evidence for the late formation of hydrous asteroids from young meteoritic carbonates. *Nat. Commun.* **3**, 627.

Gaetani G. A. and Cohen A. L. (2006) Element partitioning during precipitation of aragonite from seawater: A framework for understanding paleoproxies. *Geochim. Cosmochim. Acta* **70**, 46174634.

Grady M. M., Wright I. P., Swart P. K. and Pillinger C. T. (1988) The carbon and oxygen isotopic composition of meteoritic carbonates. *Geochim. Cosmochim. Acta* **52**, 2855–2866.

Guo W. and Eiler J. M. (2007) Temperatures of aqueous alteration and evidence for methane generation on the parent bodies of the CM chondrites. *Geochim. Cosmochim. Acta* **71**, 5565–5575.

Hanowski N. P. and Brearley A. J. (2001) Aqueous alteration of chondrules in the Cm carbonaceous chondrite, Allan Hills 81002: Implications for parent body alteration. *Geochim. Cosmochim. Acta* **65**, 495518.

Hardie L. A. (1996) Secular variation in seawater chemistry: An explanation for the coupled secular variation in the mineralogies of marine limestones and potash evaporites over the past 600 m.y. *Geology* **24**, 279–283.

Hövelmann J., Austrheim H., Beinlich A. and Munz I. A. (2011) Experimental study of the carbonation of partially serpentinized and weathered peridotites. *Geochim. Cosmochim. Acta* **75**, 67606779.

Huang Y. and Fairchild I. J. (2001) Partitioning of Sr^{2+} and Mg^{2+} into calcite under karst-analogue experimental conditions. *Geochim. Cosmochim. Acta* **65**, 4762.

Jenniskens P., Fries M. D., Qing-Zhu Y., Zolensky M., Krot A. N., Sanford S. A., Sears D., Bauford R., Ebel D. S., Friedrich J. M., Nagashima K., Wimpenny J., Yamakawa A., Nishiizumi K., Hamajima Y., Caffee M., Weten K. C., Laubenstein M., Davis A., Simon S. B., Heck P. R., Young E. D., Kohl I. E., Thimens M. H., Nunn M. H., Mikouchi T., Hagiya K., Ohsumi K., Cahill T. A., Lawton J. A., Barnes D., Steele A., Rochette P., Verosub K. L., Gattacceca J., Cooper G., Glavin D. P., Burton A. S., Dworkin J. P., Elsila J. E., Pizzerello S., Ogliore R., Schitt-Kopplin P., Harir M., Hertkorn N., Verchovsky S., Grady M., Nagao K., Okazaki R., Takechi H., Hirori T., Smith K., Silber E. A., Brown P. G., Albers J., Klotz D., Hankey M., Matson R., Fries J. A., Walker R. J., Puchtel I., Lee C.-T. A., Erdman M. E., Eppich G. R., Roeske S., Gabelica Z., Lerche M., Nuevo M., Girten B. and Worden S. P. (2012) Radar-enabled recovery of the Sutter's Mill meteorite, a carbonaceous chondrite regolith breccia. *Science* **338**, 1583–1587.

Johnson C. A. and Prinz M. (1993) Carbonate compositions in CM and CI chondrites, and implications for aqueous alteration. *Geochim. Cosmochim. Acta* **57**, 28432852.

Kelemen P. B., Matter J., Streit E. E., Rudge J. F., Curry W. B. and Blusztajn J. (2011) Rates and mechanisms of mineral carbonation in petidotite: Natural processes and recipes for enhanced, in situ CO_2 capture and storage. *Annu. Rev. Earth Planet. Sci.* **39**, 545576.

Kim S.-T., O'Neil J. R., Hillaire-Marcel C. and Mucci A. (2007) Oxygen isotope fractionation between synthetic aragonite and water: Influence of temperature and Mg^{2+} concentration. *Geochim. Cosmochim. Acta* **71**, 47044715.

Kohl I. E., Yin Q. Z. and Young E. D. (2013) Sutter's Mill meteorite oxygen isotopes: More evidence for water-rock open system alteration. *Lunar Planet. Sci. 44*. Lunar Planet. Inst., Houston. #13005 (abstr.).

Lee M. R. (1993) The petrography, mineralogy and origins of calcium sulphate within the Cold Bokkeveld CM carbonaceous chondrite. *Meteoritics* **28**, 5362.

Lee M. R. and Ellen R. (2008) Aragonite in the Murray (CM2) carbonaceous chondrite: Implications for parent body compaction and aqueous alteration. *Meteorit. Planet. Sci.* **43**, 1219–1231.

Lee M. R., Lindgren P., Sofe M., Alexander C. M. O'D. and Wang J. (2012) Extended chronologies of aqueous alteration in the CM2 carbonaceous chondrites: Evidence from carbonates in Queen Alexandra Range 93005. *Geochim. Cosmochim. Acta* **92**, 148–169.

Lindgren P., Lee M. R., Sofe M. R. and Burchell M. J. (2011) Microstructure of calcite in the CM2 carbonaceous chondrite LON 94101: Implications for deformation history during and/or after aqueous alteration. *Earth Planet. Sci. Lett.* **306**, 289–298.

Lindgren P., Lee M. R. and Sofe M. (2012) Evidence for multiple fluid pulses in the CM1 carbonaceous chondrite parent body. *Lunar Planet. Sci. 43*. Lunar Planet. Inst., Houston. #1949 (abstr.).

Lindgren P., Lee M. R., Sofe M. R. and Zolensky M. E. (2013) Clasts in the CM2 carbonaceous chondrite Lonewolf Nunataks 94101: Evidence for aqueous alteration prior to complex mixing. *Meteorit. Planet. Sci.* **48**, 1074–1090.

Maeda M., Tomeoka K. and Seto Y. (2009) Early aqueous alteration in the QUE97990 and Y791198 CM carbonaceous chondrites. *J. Mineral. Petrol. Sci.* **104**, 92–96.

Matter J. M. and Kelemen P. B. (2009) Permanent storage of carbon dioxide in geological reservoirs by mineral carbonation. *Nat. Geosci.* **2**, 837841.

Morse J. W., Wang Q. and Tsio M. Y. (1997) Influences of temperature and Mg:Ca ratio on $CaCO_3$ precipitates from seawater. *Geology* **25**, 85–87.

Müller W. F., Kurat G. and Kracher A. (1979) Chemical and crystallographic study of cronstedite in the matrix of the Cochabamba (CM2) carbonaceous chondrite. *Tschermaks Min. Pet. Mitt.* **26**, 293–304.

Palguta J., Schubert G. and Travis B. J. (2010) Fluid flow and chemical alteration in carbonaceous chondrite parent bodies. *Earth Planet. Sci. Lett.* **296**, 235–243.

Parsons I. and Lee M. R. (2009) Mutual replacement reactions in alkali feldspars I: Microtextures and mechanisms. *Contrib. Miner. Petrol.* **157**, 641–661.

Putnis A. (2002) Mineral replacement reactions: From macroscopic observations to microscopic mechanisms. *Mineral. Mag.* **66**, 689–708.

Redfern S. A. T., Salje E. and Navrotsky A. (1989) High-temperature enthalpy at the orientational order-disorder transition in calcite: Implications for the calcite/aragonite phase equilibrium. *Contrib. Miner. Petrol.* **101**, 479–484.

Riciputi L. R., McSween, Jr., H. Y., Johnson C. A. and Prinz M. (1994) Minor and trace element concentrations in carbonates of carbonaceous chondrites, and implications for compositions of co-existing fluids. *Geochim. Cosmochim. Acta* **58**, 13431351.

Rubin A. E. (2012) Collisional facilitation of aqueous alteration in CM and CV carbonaceous chondrites. *Geochim. Cosmochim. Acta* **90**, 181–194.

Rubin A. E., Trigo-Rodriguez J. M., Huber H. and Wasson J. T. (2007) Progressive aqueous alteration of CM carbonaceous chondrites. *Geochim. Cosmochim. Acta* **71**, 2361–2382.

Sofe M. R. (2013) The oldest carbonate minerals on Earth: Insights into the early history of the Solar System. Unpublished Ph. D. thesis, Univ. Glasgow.

Sofe M. R., Lee M. R. and Lindgren P. (2011) Aragonite in the CM carbonaceous chondrites: A proxy for the magnitude of aqueous alteration. *Meteorit. Planet. Sci.* **46** (abstr. no. 5250).

Starkey N. A. and Franchi I. A. (2013) Insight into the silicate and organic reservoirs of the comet forming region. *Geochim. Cosmochim. Acta* **105**, 73–91.

Threlfall T. (2003) Structural and thermodynamic explanations of Ostwald's rule. *Org. Process Res. Dev.* **7**, 1017–1027.

Tomeoka K. and Buseck P. R. (1985) Indicators of aqueous alteration in CM carbonaceous chondrites: Microtextures of a layered mineral containing Fe, S, O, and Ni. *Geochim. Cosmochim. Acta* **49**, 21492163.

Travis B. J. and Schubert G. (2005) Hydrothermal convection in carbonaceous chondrite parent bodies. *Earth Planet. Sci. Lett.* **240**, 234250.

Tyra M. A., Farquhar J., Wing B. A., Benedix G. K., Jull A. J. T., Jackson T. and Thiemens M. H. (2007) Terrestrial alteration of carbonate in a suite of Antarctic CM chondrites: Evidence from oxygen and carbon isotopes. *Geochim. Cosmochim. Acta* **71**, 782–795.

Tyra M. A., Farquhar J., Guan Y. and Leshin L. A. (2012) An oxygen isotope dichotomy in CM2 chondritic carbonates—A SIMS approach. *Geochim. Cosmochim. Acta* **77**, 383–395.

White S. N. (2009) Laser Raman spectroscopy as a technique for identification of seafloor hydrothermal and cold seep minerals. *Chem. Geol.* **259**, 240–252.

Young E. D. (2001) The hydrology of carbonaceous chondrite parent bodies and the evolution of planet progenitors. *Philos. Trans. R. Soc. London A* **359**, 2095–2110.

Young E. D., Ash R. D., England P. and Rumble, III, D. (1999) Fluid flow in chondritic parent bodies: Deciphering the compositions of planetesimals. *Science* **286**, 1331–1335.

Young E. D., Zhang K. K. and Schubert G. (2003) Conditions for pore water convection within carbonaceous chondrite parent bodies – implications for planetesimal size and heat production. *Earth Planet. Sci. Lett.* **213**, 249–259.

Zolensky M. E., Barrett R. and Browning L. (1993) Mineralogy and composition of matrix and chondrule rims in carbonaceous chondrites. *Geochim. Cosmochim. Acta* **57**, 3123–3148.

Associate editor: Christian Koeberl